

# A First-Principles Computational Framework for Liquid Mineral Systems

B.B. Karki<sup>1</sup>, D. Bhattarai<sup>1</sup> and L. Stixrude<sup>2</sup>

**Abstract:** Computer modeling of liquid phase poses tremendous challenge: It requires a relatively large simulation size, long simulation time and accurate interatomic interaction and as such, it produces massive amounts of data. Recent advances in hardware and software have made it possible to accurately simulate the liquid phase. This paper reports the details of methodology used in the context of liquid simulations and subsequent analysis of the output data. For illustration purpose, we consider the results for the liquid phases of two geophysically relevant materials, namely MgO and MgSiO<sub>3</sub>. The simulations are performed using the parallel first-principles molecular dynamics (FPMD) technique within the framework of density functional theory. Various physical properties including the equation of state, diffusion, atomic structure and electronic structure of these liquids are obtained as a function of pressure and temperature. The three-dimensional and time-dependent data for atomic configuration and electronic density are analyzed using the recently developed space-time-multiresolution and multiple-dataset-visualization techniques. It is shown that the structural, dynamical and electronic properties of the liquid phases are highly sensitive to compression, with no discernible influence of temperature in most cases.

**keyword:** Parallel simulation, Visualization, First-principle approach, Minerals.

## 1 Introduction

Understanding the behavior of the liquid state of ceramics and minerals has long been the subject of considerable interest as well tremendous challenge for computational scientists. In a solid phase, the constituent atoms interact strongly with each other and often form a crystalline (perfectly ordered) structure. As such, most crys-

talline properties can be modeled using unit cell containing a relatively few atoms thereby exploiting the crystal symmetry to a great extent. This is no longer true in the case of a liquid phase: The constituent atoms still interact strongly with each other, however, they do not form any long-range correlations. Even the short-range (local) order is temporal and transient fluctuations also occur in the liquid phase.

The temporal (dynamical) nature of the liquid state, which can be only described by statistical measures, requires the construction of accurate and representative ensembles [Allen and Tildesley (1987)]. This implies two important concerns: First, the ensemble should contain accurate interatomic interactions. Unlike the crystalline phase, it is not straightforward to generate empirical interaction potential that can correctly capture the dynamic nature of the liquid state. In this sense, it is natural to prefer to derive the required interactive forces from a quantum mechanical treatment. The resulting approach can be called the first-principles molecular dynamics (FPMD) method, in contrast to the traditional molecular dynamics method, which being based on either empirical or simplified force field model has widely been used to simulate a variety of materials problems [e.g., Cohen and Gong (1994), Belonoshko and Subrovinsky (1996), Srivastava and Atluri (2002), Shen and Atluri (2004), Aguado and Madden (2005)]. A widely used FPMD method is based on density functional theory, which explicitly deals with electrons making it computationally very intensive [Hohenberg and Kohn (1964), Kohn and Sham (1965)]. Second, the representative ensemble must be sufficiently large. Supercells with periodic boundary conditions containing a relatively large number of atoms are commonly used to replicate an ensemble for the liquid state. The system sizes from several tens to a few hundreds of atoms are typical for the first-principle approach [e.g., Chelikowsky et al. (2001), Trave et al. (2002), Stixrude and Karki (2005), Alfe (2005), Karki et al. (2006)]. Also, the simulation needs to be run for relatively long time, which can range from a few to several picoseconds or even more

<sup>1</sup> Department of Computer Science, Department of Geology and Geophysics, Louisiana State University, Baton Rouge, LA 70803, U.S.A.

<sup>2</sup> Department of Geological Sciences, University of Michigan, Ann Arbor, MI 48109, U.S.A

to ensure that the time-averaged properties are well converged.

Another important issue in the modeling liquid state is related to the choice of input configuration. Two common approaches exist: The first one is to melt the crystalline phase by thermalizing it at a very high temperature, which is often chosen to be well above the corresponding melting temperature. The system is then quenched to a desired lower temperature. The other one is to generate random atomic configuration and thermalize at high temperature. In this case, the initial configuration does not retain any information of the crystalline phase and the simulations converge relatively slow.

Last important issue is related to analysis of the simulation outputs. FPMD simulations are expected to produce massive amounts of three-dimensional and time-dependent data for the atomic configuration and electron density distribution. In essence, these data represent snapshots of the atomic and electronic structures of the liquid state at different instants of time. In recent years, visualization approach has emerged as an attractive approach to uncover important, otherwise hidden information in large-scale sets of scientific data. Several visualization systems (public domain or commercial nature) such as *XCRYSDEN* [Kokaji (1999)], *VMD* [Humphrey et al. (1996)], *Atomsviwer* [Sharma et al. (2003)], *Crystalmaker*, and *Amira* are available, however, using them is always not the best choice. They may not fulfill several specific features that are needed for a successful visualization of the liquid data due to the complex spatio-temporal characteristics of the data. We have recently initiated development of two visualization schemes: They are space-time-multiresolution visualization of atomistic data [Bhattarai and Karki (2006)] and multiple-dataset-visualization of electron density [Khanduja and Karki (2006)].

In this paper, we illustrate the FPMD simulation and visualization approach for the liquid phases of two widely studied materials, namely MgO and MgSiO<sub>3</sub>. Only the results, which are relevant and/or not previously reported, are presented. Other details can be found elsewhere [Stixrude and Karki (2005), Karki et al. (2006)]. These systems were previously studied using methods based on empirical or simplified potential models [e.g., Cohen and Gong (1994), Belonoshko and Subrovinsky (1996), Aguado and Madden (2005)]. There are several reasons behind this motivation. First, they are thought to

be the most abundant phases in Earth's mantle. Knowledge of their liquid properties under extreme pressure and temperature conditions of the deep interior is essential to modeling the thermal, chemical and dynamical state of the Earth. For instance, the equation of state of the liquid is an important factor controlling the relative density of partial melts produced by geological processes and co-existing solids, and thus whether these melts will rise or sink [Rigden et al. (1984)]. The diffusivity controls the rate of chemical reaction of liquids with their surroundings, and can be related to the viscosity, which controls the rate of transport. Second, understanding the physics of these liquids is expected to lend considerable insight into the behavior of other oxide and silicate liquids. Third, relevant experimental studies are still lacking so the FPMD approach can be considered as an attractive complement to experiment. For instance, the only available experimental data relevant to the high-pressure liquid phase are for melting up to some moderate pressure [Zerr and Boehler (1994)].

The organization of the paper is as follows: The Section 2 presents the methodology in the context of parallel computation and visualization. The Section 3 presents the specific results such as the equation of state, correlation function and diffusion coefficient. The simulation data for atomic and electronic structures are visualized in the Section 4. Finally, the Section 5 draws some conclusions.

## 2 Methodology

### 2.1 Parallel computation

Computations are performed using the first-principles molecular dynamics (FPMD) method. The corresponding parallel program is called VASP [Kresse and Furthmuller (1996)], which has been implemented with a Fortran90 and Message Passing Interface (MPI). It exploits dynamic memory allocation and a single executable, which can be used to simulate a wide range of calculations. The execution times of the VASP code are examined on the 1024 Xeon processor Linux Cluster (called *Supermike*) of Louisiana State University. For a 64-atom system, the average execution time per FPMD step is about 12 seconds with 32 CPUs used. For a 216-atom system, the time is about 95 seconds with 128 CPUs used.

The interatomic forces in the FPMD approach are of quantum origin, which are calculated using density func-

tional theory [Hohenberg and Kohn (1964), Kohn and Sham (1965)]. The forces are computed at each time step of the simulation from a fully self-consistent solution of the electronic structure problem represented by the well-known Kohn-Sham equation:

$$\left[ \frac{\hbar^2}{2m} \nabla^2 + V_n(\vec{r}) + V_H(\vec{r}, \rho(\vec{r})) + V_{XC}(\vec{r}, \rho(\vec{r})) \right] \psi_i(\vec{r}) = \epsilon_i \psi_i(\vec{r})$$

Here, the first-term is the kinetic energy,  $V_n$  is the ion-electron potential,  $V_H$  is the Hartree potential (Coulomb interaction among electrons) and  $V_{XC}$  is the exchange-correlation potential (all many-body effects). The electron charge density is given by  $\rho(\vec{r}) = \sum_i |\psi_i(\vec{r})|^2$ . The local density approximation is used to represent  $V_{XC}$  [Ceperley and Alder (1980)]. Ultrasoft Mg (with the core radius of 1.06 Å and the  $3s^2$  electronic configuration), Si (0.82 Å and  $3s^2 3p^4$ ) and O (0.82 Å and  $2s^2 2p^4$ ) pseudopotentials [Kresse et al. (1992)] are used to represent  $V_n$ . A plane wave cutoff of 400 eV and gamma point sampling are used for both the solid and liquid phases.

Our FPMD approach uses the canonical ( $NVT$ ) ensemble in which the number of atoms in the periodically repeated unit cell ( $N$ ), the volume ( $V$ ), and the temperature ( $T$ ) are fixed. Temperature is controlled using an extended Lagrangian formulation in which a degree of freedom is included to represent a reservoir (thermostat) [Nose (1984)]. The Lagrangian is

$$L = \frac{1}{2} \sum_i m_i |v_i|^2 - V(\vec{r}_i) + \frac{1}{2} Q \dot{s}^2 - (f+1) k_B T_0 \ln s$$

where  $s$  is the new dynamical variable, and  $Q$  is the associated mass parameter.  $T_0$  is the externally set temperature and  $f$  is the number of degrees of freedom in the system. To speed convergence,  $Q$  is chosen so that the period of oscillation of the temperature (or  $s$ ) is similar to the mean period of atomic vibrations. Our  $NVT$  ensemble consists of 64 and 216 atoms for MgO and 80 atoms for MgSiO<sub>3</sub> in a cubic supercell.

The simulation schedules used can be described as follows: In the case of a 216-site MgO system, the crystalline structure of a given volume is first melted and equilibrated at 10,000 K for a period of 3 picoseconds. The simulation time of 3 ps means 3,000 FPMD steps, each time step being 1 fs. The system is then quenched to a desired lower temperature, say 7000 K, over a time

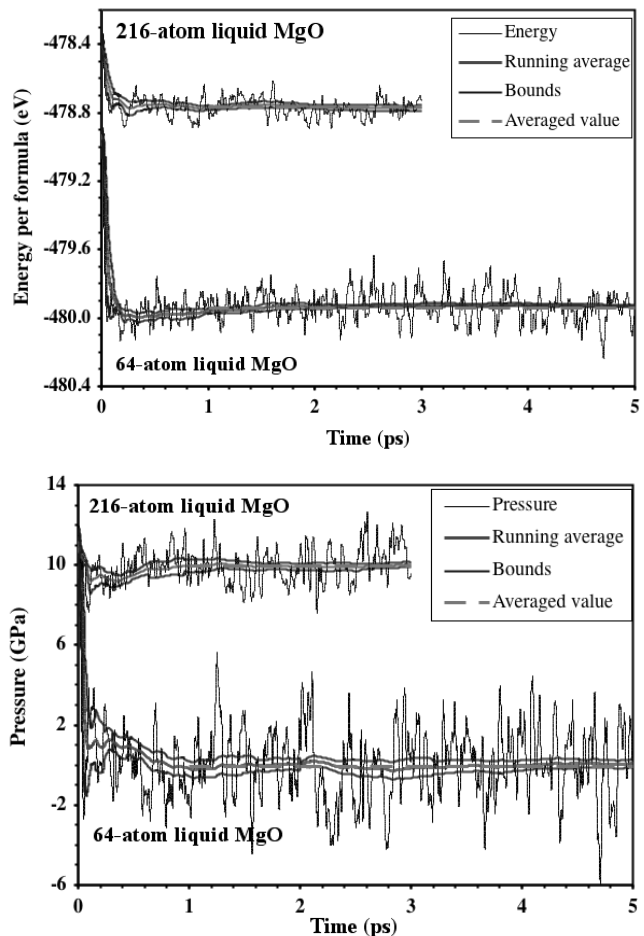


**Figure 1** : Energy-time (top) and pressure-time (bottom) series for two liquid MgO supercells. Running time-average, bounds and the averaged values are shown.

interval of 2 ps. At this temperature, we first thermalize the system for 1 ps and collect data over another 2 ps. For a smaller MgO system containing atoms, a longer simulation time of 5 ps is used. The temperature is decreased in this way to simulate the liquid at subsequent lower temperatures. The whole process is repeated at every other volume. A similar schedule with 6,000 K as a starting temperature and 3 ps as a simulation time per run is used for MgSiO<sub>3</sub>. A series of FPMD runs are conducted at several volumes along several isotherms. For each temperature-volume condition, we confirm that the system is in the liquid state by analysis of the radial distribution function and the mean-square displacement as a function of time [Allen and Tildesley (1987)]. Figure 1 shows the running time-averages of the energy and pressure for 216- and 64-site liquid MgO systems at 3000 K

converges very well over the period of 3 and 5 ps, respectively. The sizes of fluctuations are smaller for the bigger system. Uncertainties in the energy and pressure were computed by the blocking method [Flyvbjerg and Petersen (1989)].

## 2.2 Visualization

Simulations involve as many as 216 atoms and 864 electrons in MgO and 80 atoms and 384 electrons in MgSiO<sub>3</sub>, which are distributed in a three-dimensional space. Moreover, the distributions vary over time as dictated by FPMD simulation consisting of several thousands (3,000 to 5000) of steps per run. This results in massive three-dimensional and time-dependent datasets for atomic configuration and electron density. Here, we exploit the visualization approach. It uses two recently developed visualization techniques, which are space-time-multiresolution visualization of atomic position-time series and multiple-dataset-visualization of electron density volume data. Their basic features are presented below.

We use a scheme to support interactive visualization at space-time multiresolution of the atomistic simulation data [Bhattarai and Karki (2006)]. This scheme adopts two perspectives that differ in their purposes and in the way they process and render the data. First, the complete or nearly complete dataset is rendered using animation, particle-pathline and color-mapped-dimension techniques to achieve an overall idea of the spatio-temporal behavior of the atomic system under consideration. Second, additional data are generated on the fly and analyzed/visualized using a combined graph-theoretic and statistical approach to gain better and more detailed insight into the desired spatio-temporal information. The primary goal is to deal with the today's moderate-sized datasets of high accuracy produced by FPMD simulations. For this purpose, instead of just focusing on direct rendering of the given data, additional data (containing more quantitative information) that usually have to be extracted by some other means are extracted and rendered on the fly. This allows us to gain better insight at multi space-time details of the data (in other words, to extract the global as well local spatio-temporal behavior) for important information such as bonding, coordination, clustering, structural stabilities, defects, diffusion and other dynamic processes.

The second visualization scheme used deals with simul-

taneous visualization of multiple sets of data with current focus on the electron density data [Khanduja and Karki (2006)]. Multiple datasets may represent multiple samples, or multiple conditions, or multiple simulation times. Multiple dataset visualization (MDV) allows us to better understand important relationships and differences among different datasets. It has to handle and render massive amounts of data concurrently. It supports two standard visualization techniques, namely, isosurface extraction [Lorenson and Cline (1987)] and texture-based rendering [Cabral et al. (1994)] for multiple sets of the scalar volume data. Preliminary tests performed using up to 25 sets of moderate-sized ( $256^3$ ) data have shown that both techniques are no longer be interactive with the frame-rates dropping below one for six or more datasets. To improve the MDV frame-rate, a scheme based on the combination of hardware-assisted texture mapping and general clipping has been proposed. This exploits the 3D surface texture mapping by rendering only the externally visible surfaces of all volume datasets at a given instant, with dynamic clipping enabled to explore the interior of the data [Weiskopf et al. (2003), Khanduja and Karki (2005)].

## 3 Simulation results

### 3.1 Equations of state

A series of pressure-volume-temperature (PVT) data is obtained for each liquid studied covering the realistic pressure-temperature conditions of the Earth's mantle. It is important to have an accurate equation of state (EoS) representation for these data so that several thermodynamic properties of interest such as thermal expansivity, bulk modulus, thermal Gruneisen parameter, etc. can be derived from this equation. We show that the liquid data can accurately be described with the Mie-Grüneisen form:

$$P(V, T) = P(V, T_0) + P_{TH}(V, T)$$

Here,  $P(V, T_0)$  is the pressure on the reference isotherm ( $T = T_0$ ), which can be described by the third-order Birch-Murnaghan EoS [Birch (1952)]:

$$P(V, T_0) = 3K_0 f(1 + 2f)^{5/2} \left[ 1 + \frac{3}{2}(K'_0 - 4) \right]$$

where  $f = \frac{1}{2} \left[ \left( \frac{V_0}{V} \right)^{2/3} - 1 \right]$  refers to compression (the negative of the strain). For the liquid MgO, the EoS pa-

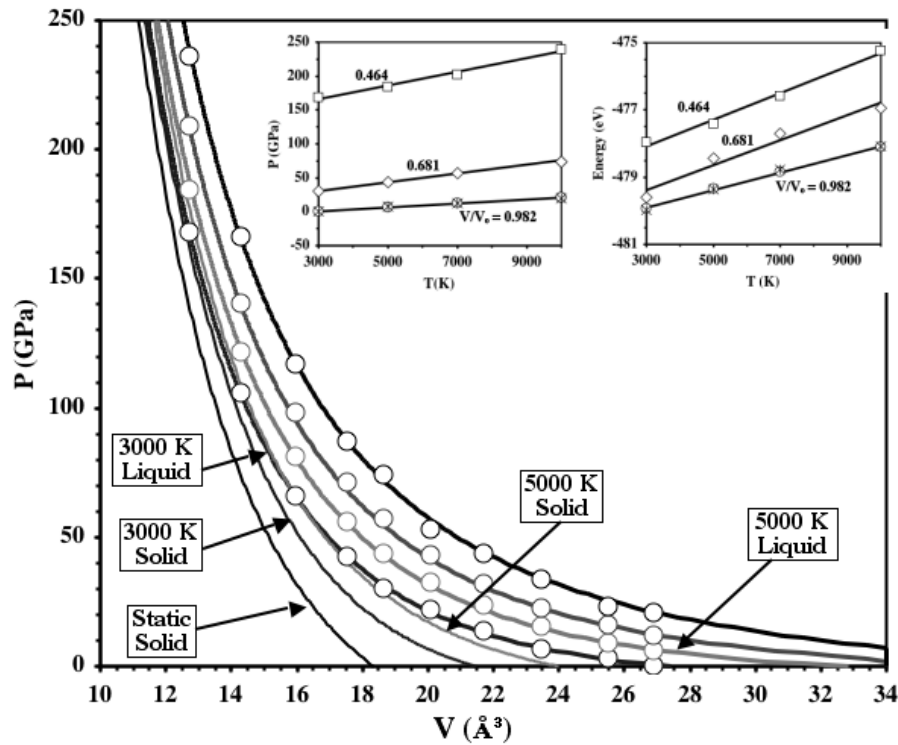


**Figure 2** : Equation of state isotherms of liquid MgO at 3000 K (blue), 5000 K (green), 7000 K (red) and 10000 K (black). The uncertainties are within the size of the symbols. The insets show the temperature variation of the total pressure and energy at selected volumes. Crosses are the data for 216-atom system. The energy at  $V/V_0 = 0.681$  is shifted up by 1 eV for the clarity.

parameters are  $T_0=3000$  K,  $V_0 = 27.40\text{\AA}^3/\text{MgO}$ ,  $K_0 = 30.8$  GPa and  $K'_0 = 5.03$  [Karki et al. (2006)]. The corresponding parameters for the silicate liquid are  $T_0=3000$  K,  $V_0 = 72.99\text{\AA}^3/\text{MgSiO}_3$ ,  $K_0 = 10.1$  GPa and  $K'_0 = 7.6$  [Stixrude and Karki (2005)]. Both the thermal pressure and internal energy are shown to be linear in temperature at each volume (Insets of Figure 2).

The calculated  $PVT$  results along with EoS fits for liquid MgO are shown in Figure 2. The isotherms systematically diverge on compression. This is due to the fact that the thermal pressure increases on compression. The volume difference between the solid and liquid phase is shown to decrease with compression. For MgO, the volume difference for the 3000 K isotherm is  $5.79\text{\AA}^3$  at zero pressure, and  $0.15\text{\AA}^3$  at 150 GPa. We have also calculated the coefficient of thermal expansivity, which is defined by  $\alpha = \frac{1}{V} \frac{\partial V}{\partial T}$ . The value of  $\alpha$  is  $9.12 \times 10^{-5} \text{K}^{-1}$  at zero pressure and  $T = 5000$  K. With increasing pressure, it decreases rapidly reaching  $1.68 \times 10^{-5} \text{K}^{-1}$  at 150 GPa and  $T = 5000$  K. Similarly, using the predicted temper-

ature variations of the thermal pressure and energy, one can compute the constant volume heat capacity defined by  $C_V = \frac{\partial E}{\partial T}$  and the thermal Gruneisen parameter defined by  $\gamma = \frac{V}{C_V} \frac{\partial P_{TH}}{\partial T}$ , see Stixrude and Karki (2005) and Karki et al. (2006).

### 3.2 Radial distribution function

The radial distribution function (RDF),  $g(r)$ , is computed to examine the structural properties of the simulated liquid system [Allen and Tildesley (1987)]. The RDF is the probability of finding another atom at a distance  $r$  from a specified atom. Here, we show three partial Mg-O, Mg-Mg and O-O RDFs for the oxide liquid (Figure 3, top) and five partial Mg-O, Mg-Mg, Mg-Si, Si-Si, Si-O and O-O RDFs for the silicate liquid (Figure 3, bottom). In each case, the RDF exhibits large fluctuations at small distances and approaches unity at larger distances indicating the short-range order and long-range disorder characteristic of the liquid state. The first peak decreases in amplitude and its position systematically shifts to a

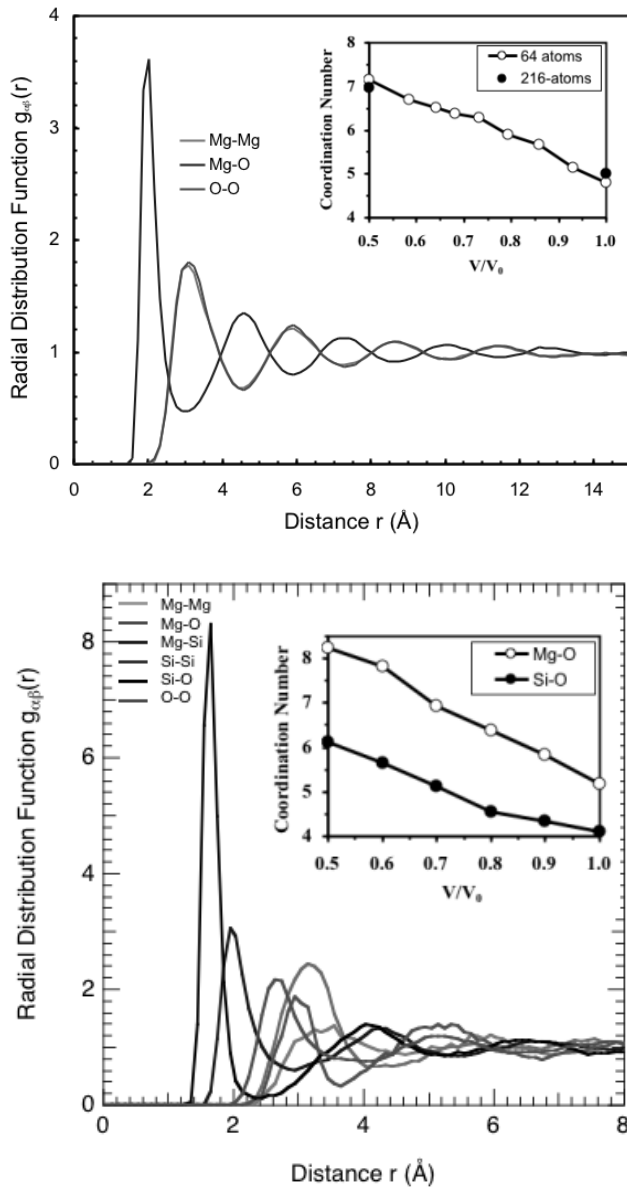


**Figure 3** : Radial distribution function for the oxide liquid at  $V/V_0 = 0.982$  and 3000 K (top) and the silicate liquid at  $V/V_0 = 0.885$  and 3000 K (bottom). The inset shows the temperature-averaged Mg-O and Si-O coordination numbers as a function of volume.

smaller distance as the compression increases.

The average coordination numbers is calculated using:

$$C_{\alpha\beta} = 4\pi\rho x_{\beta} \int_0^{r_{\min}} r^2 g_{\alpha\beta}(r) dr$$

Here,  $\rho$  is the number density and  $x_{\beta}$  is the concentra-

tion ( $N_{\beta}/N$ ) of species  $\beta$ . The cutoff is taken to be the first minimum ( $r_{\min}$ ) of the corresponding partial pair distribution function. The calculated average Mg-O coordination number from the 216-atom liquid MgO is 5 and 7 at zero and high pressures, which are smaller than the crystalline coordination of 6. This agrees with the 64-atoms simulation [Karki et al. (2006)], which shows that the coordination number increases with increasing pressure and exceeds 7 at pressures above 150 GPa (Inset of Figure 3, top). For MgSiO<sub>3</sub>, the calculated average Mg-O and Si-O coordination numbers increase smoothly and nearly linearly with compression from 6 and 4, respectively, at low pressure, to 8 and 6, respectively, at high pressure (Inset of Figure 3, bottom). The effects of temperature, however, do not show any systematic trend [Stixrude and Karki (2005), Karki et al. (2006)].

### 3.3 Diffusion coefficient

Diffusion is an important dynamical phenomenon for a liquid phase. It can be characterized by calculating diffusion coefficient as follows

$$D = \lim_{t \rightarrow \infty} \frac{\langle [r(t)]^2 \rangle}{6t}$$

where

$$\langle [r(t)]^2 \rangle = \frac{1}{N} \sum_{i=1}^N |\vec{r}_i(t+t_0) - \vec{r}_i(t_0)|^2$$

is the mean square displacement (MSD), and  $\vec{r}_i(t_0)$  and  $\vec{r}_i(t+t_0)$  are the positions of  $i^{\text{th}}$  atom at the start and end of the time interval  $t$ . The MSD for a given time  $t$  is then calculated by averaging over time origins ( $t_0$ ). The MSD is shown to be nearly linear with time in each case (Figure 4). The calculated total self-diffusion coefficients are fit to the Arrhenius relation:

$$D(P, T) = D_0 \exp[-(E_a + PV_a)/RT]$$

with  $D_0 = 200 \text{ m}^2/\text{s}$ ,  $E_a = 0.85 \text{ eV}$  is the activation energy, and  $V_a = 1.3 \text{ \AA}^3$  is the activation volume for liquid MgO. The results show that temperature systematically enhances diffusion whereas pressure systematically suppresses it in both liquids (Figure 5). The partial diffusion coefficient for O atoms is on average larger than that for Mg and Si atoms.

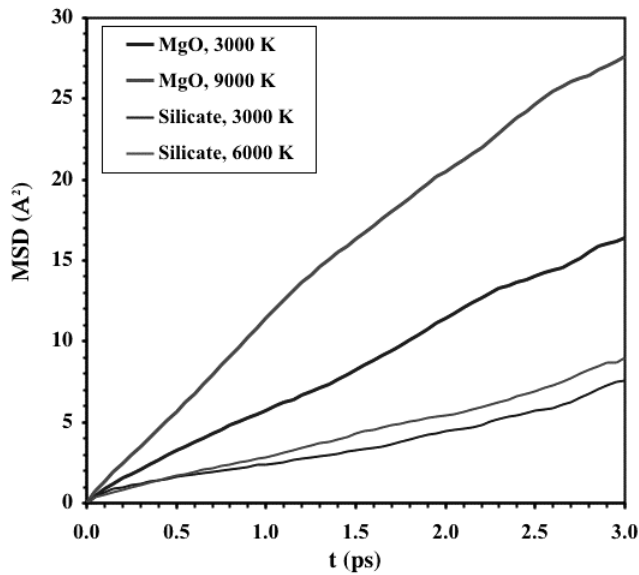


**Figure 4** : Total mean square displacement (MSD) as a function of time. Oxide liquid at  $V/V_0 = 0.982$  and 3000K, and  $V/V_0 = 0.522$  and 9000K. Silicate liquid at  $V/V_0 = 0.885$  and 3000 K, and  $V/V_0 = 0.442$  and 6000 K.

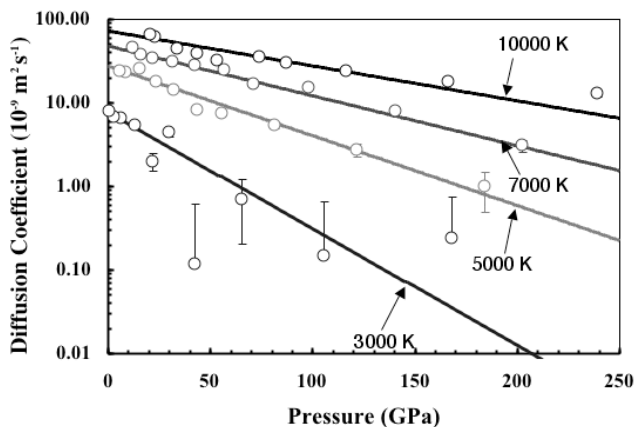


**Figure 5** : Diffusion coefficient (symbols) as a function pressure and temperature and the fit (lines) to the Arrhenius law for the liquid MgO.

## 4 Visualization of the data

### 4.1 Atomistic structure

The liquid structure is analyzed here by performing visualization of the atomic coordination environment although other properties such as the nearest-neighbors, common-neighbors, structural units (such as polyhedra)

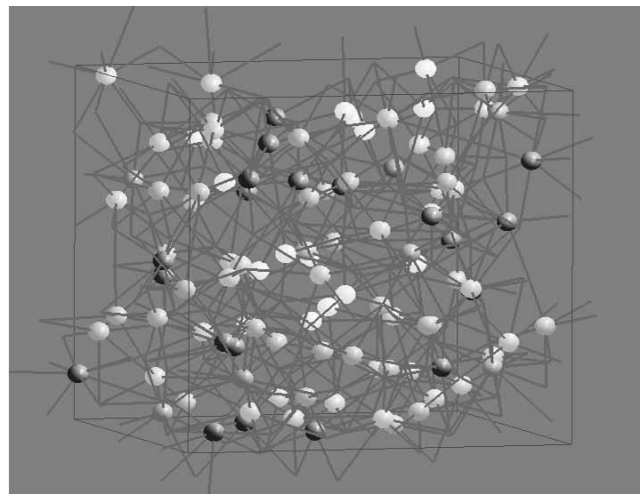
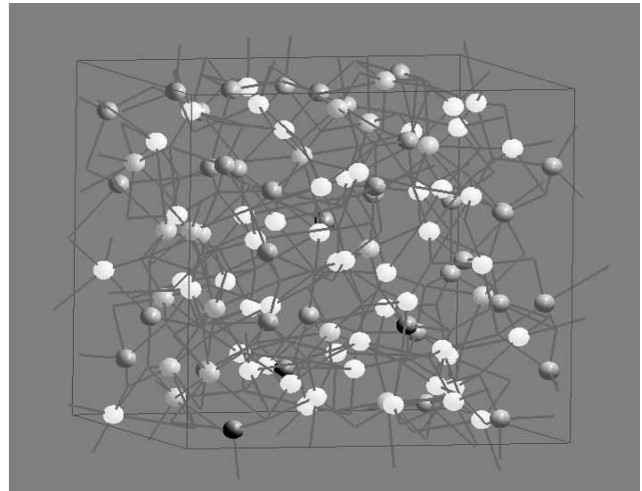


**Figure 6** : Visualization of Mg-O coordination environment in a 216-atom liquid MgO system. Top: low compression ( $V/V_0 = 0.982$ ) and 3000 K. Bottom: high compression ( $V/V_0 = 0.522$ ) and 9000K. Only Mg atoms are shown. See the text for the color interpretation.

and their stability and distortion, atomic displacement can also be visualized. The spatial variation of Mg-O coordination as a function of time in the MgO liquid (Figure 6) and that of Si-O coordination in the silicate liquid (Figure 7) are visualized. The coordination-encoded spheres and Si-O polyhedra are used to render the coordination environment. A RGB (red, green and blue) cubic color map is used to encode the calculated atomic coordination number (CN): The RGB values of (0,0,0), (1,0,0), (1,1,0), (0,1,0), (0,1,1), (0,0,1) and (1,1,1), which translate to the colors of black, red, yellow, green, cyan, blue,

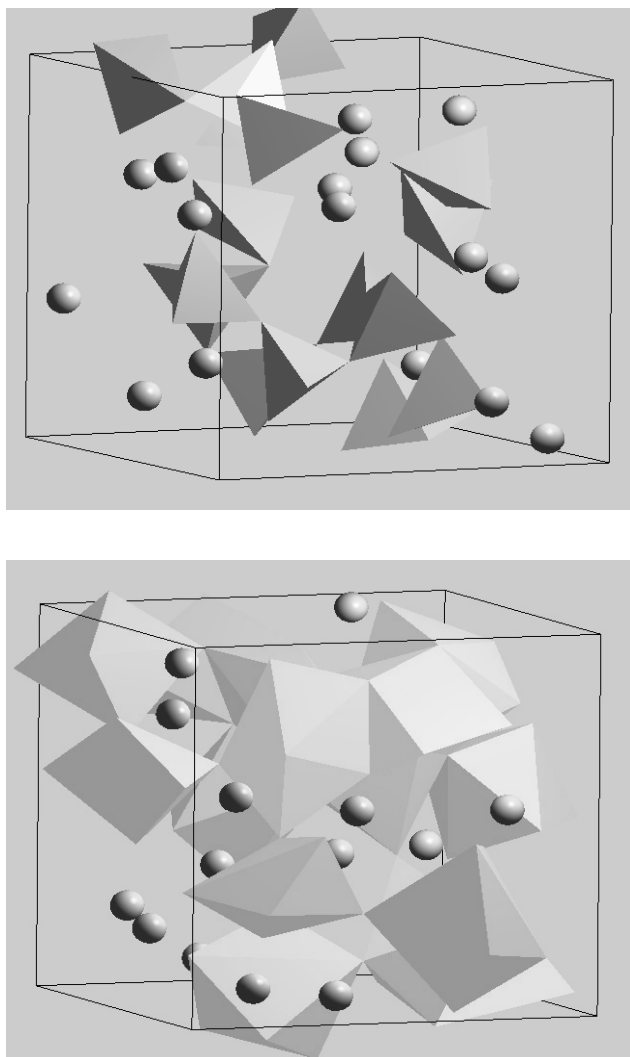


**Figure 7** : Visualization of Si-O coordination environment in liquid  $\text{MgSiO}_3$ . Top: low compression ( $V/V_0 = 0.885$ ) and 3000 K. Bottom: high compression ( $V/V_0 = 0.442$ ) and 6000 K.

magenta and white, respectively, are for the CN values of  $\leq 3$ , 4, 5, 6, 7, 8, 9 and  $\geq 10$ , respectively. The visualization outputs imply that the coordination is not uniform in space and relative contributions of different types (which range from 3-fold to 10-fold) of coordination vary to some extent over the time.

Out of 108 Mg atoms of the 216-atom liquid MgO system, there are 4 three- (black), 37 four- (red), 49 five- (yellow), 17 six- (green) and 1 seven- (cyan) fold coordinated Mg atoms at zero pressure (Figure 6, top). The CN distribution is found to vary much more with compres-

sion than with temperature. At high pressure, there are 1 four- (red), 15 five- (yellow), 31 six- (green), 36 seven- (cyan), 19 eight- (blue) and 6 nine- (magenta) fold coordinated Mg atoms (Figure 6, bottom). Visualization reveals that compression increasingly suppresses the low-CN contributions (3-, 4- and 5-fold coordination) and enhances high-CN contributions (6-, 7- and 8-fold coordination).

At zero pressure, the  $\text{MgSiO}_3$  liquid shows mostly four-fold Si-O coordination, which is characteristic to the corresponding crystalline pyroxene phase. Visualization output (Figure 7, top) contains 15 red (four-fold) and 1 yellow (five-fold) polygons. Note that there is a total of 16 Si-polyhedra in the 80-atom system. However, the liquid structure lacks the elements of longer ranged order seen in the crystal and isolated polyhedra exist. With increasing compression the number of four-fold coordination decreases whereas the number of five- and six-fold coordination increases. At high pressure, the Si-O coordination is mostly six-fold, which is characteristic of the corresponding crystalline perovskite phase (Horiuchi et al. (1987)). There are 12 green (six-fold), 1 yellow (five-fold) and 3 cyan (seven-fold) polyhedra, see Figure 7, bottom. Visualization also reveals that polyhedron remain connected to each other, however, they do not form a complete 3D framework of corner sharing octahedra as in the crystalline phase in which every octahedra shares its all six corners with other octahedra.

#### 4.2 Electronic structure

The calculated electronic density volume data are visualized using the multiple-dataset-visualization technique [Khanduja and Karki (2006)]. The visualization outputs are presented only for the liquid MgO data. The crystalline MgO is highly ionic in the nature [Chang and Cohen (1984)]: The valence electrons from Mg atoms along with others are primarily localized in the vicinity of O ions. As a result, the electronic distribution shows nearly spherical symmetry about each O site. The visual analysis shows that in the liquid phase, due to dynamic rearrangement of atoms, the spherical distributions are significantly perturbed. The MDV isosurfaces are extracted for two isovalues of density ( $0.05$  and  $0.15 \text{ \AA}^{-3}$ ) at two conditions (equilibrium volume and 3000 K, and compressed volume and 9000 K), shown in Figure 8. The isosurfaces at compressed volume appear to be more distorted from the ideal spherical shape.

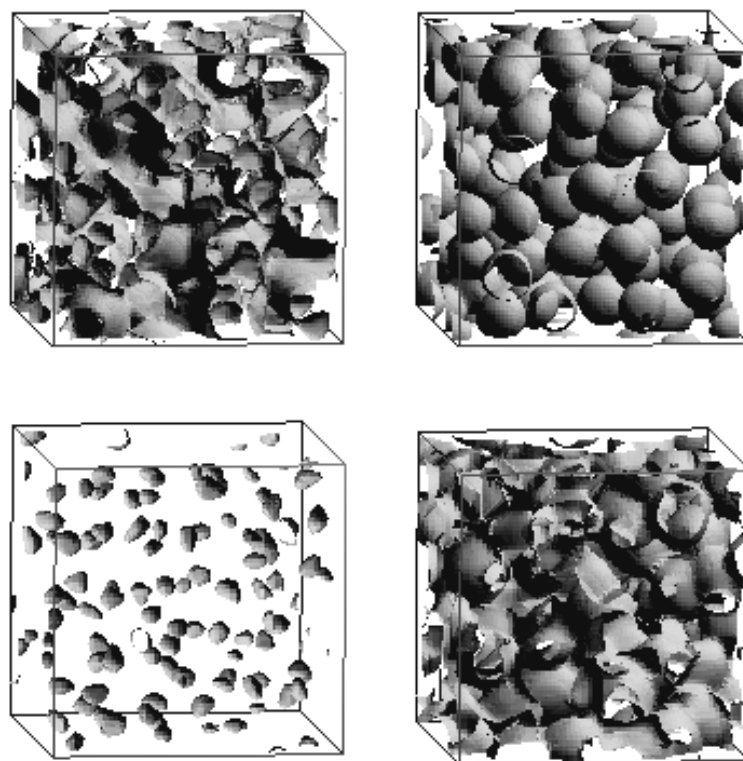


**Figure 8** : Electronic density isosurfaces at two isovalues (left:  $0.05 \text{ \AA}^{-3}$  and right:  $0.15 \text{ \AA}^{-3}$ ) at two equilibrium (top) and compressed volume (bottom).

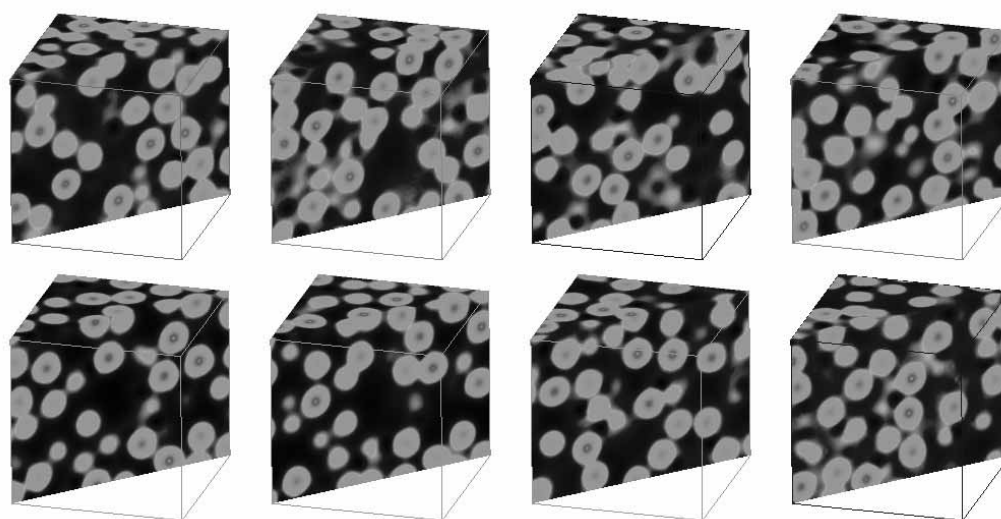


**Figure 9** : Texture 3D mapping of 8 sets of electronic density data for the 216-atom liquid MgO. From the lower left to lower right, the data correspond to temperatures of 1000, 2000, 3000 and 4000 K. Then from the upper left to upper right, the data correspond to 5000, 6000, 7000 and 10000 K.

Eight sets of data of the liquid MgO as a function of temperature at uncompressed volume are rendered using 3D surface texture mapping (Figure 9). A multiscale RGB (red, green and blue) color map is used: The B component (with  $R = 0$  and  $G = 0$ ) is first varied from 0 to 1 for the density variation from 0 to  $0.01 \text{ \AA}^{-3}$ . Then the

green component (with  $R = 0$  and  $B = 1$ ) is increased to 1 over the density range from 0.01 to 0.05  $\text{\AA}^{-3}$ . Finally, the red component is increased and both the B and G components are decreased for the density values from 0.05 to 1  $\text{\AA}^{-3}$ . One can clearly see that the electron density distribution around O ions forms inter-atomic bridges instead of forming isolated structures (red and green areas). There are some extended regions of low density (blue colored) as well. One can also see more dark regions at low temperatures than at high temperatures indicating voids at low temperatures possibly related to the structure being more ordered in some sense.

## 5 Conclusions

We have successfully illustrated the parallel first-principle molecular dynamics simulation approach for two geophysically important liquid phases, namely MgO and MgSiO<sub>3</sub>, at realistic pressure-temperature conditions of the Earth's mantle. The methodology used consisting of parallel simulation and subsequent visualization of the data is presented. It is shown that the calculated pressure-volume-temperature relationships can be well represented with the standard Mie-Grüneisen equation of state. The liquid structure is analyzed by calculating the radial distribution functions and the corresponding coordination. In particular, visualization reveals that the Mg-O and Si-O coordination environments vary substantially with compression. Finally, the electronic structure of the liquid state is visualized to show that it deviates significantly from that of the crystalline phase.

**Acknowledgement:** This work was supported by the NSF Career grant (EAR 0409074) and collaborative grant (EAR 0409074). Computing facilities were provided by CCT at Louisiana State University.

## References

- Aguado, A.; Madden, P. A.** (2005): New insights into the melting behavior of MgO from molecular dynamics simulations: the importance of premelting effects. *Physical Review Letters*, vol. 94, 68501.
- Alfe, D.** (2005): Melting curve of MgO from first-principles simulations. *Physical Review Letters*, vol. 94, 235701.
- Allen, M. J.; Tildesley, D. J.** (1987): *Computer simulation of liquids*, Oxford University Press, Oxford.
- Belonoshko A. B.; Dubrovinsky, L. S.** (1996): Molecular dynamics of NaCl (B1 and B2) and MgO (B1) melting: two-phase simulation. *American Mineralogist*, vol. 81, pp. 303-316.
- Bhattarai, D.; Karki, B. B.** (2006): Visualization of atomistic simulation data for spatio-temporal information. *The 14<sup>th</sup> Int. Conf. on Computer Graphics, Visualization and Computer Vision (WSCG 2006)*, ISBN 80-86943-03-8, pp. 17-24.
- Birch, F.** (1952): Elasticity and constitution of the Earth's interior. *J of Geophysical Research*, vol. 57, pp. 227-286.
- Cabral, B.; Cam, N.; Foran, J.** (1994): Accelerated volume rendering and tomographic reconstruction using texture-mapping hardware. *Proc. of 1994 Symposium on Volume Visualization*, pp. 91-98.
- Ceperley, D. M.; Alder, B. J.** (1980): Ground state of the electron gas by a stochastic method. *Physical Review Letters*, vol. 45, pp. 566-569.
- Chang, K. J.; Cohen, M. L.** (1984): High-pressure behavior of MgO: structural and electronic properties. *Physical Review B*, vol. 30, pp. 4774-4781.
- Chelikowsky, J. R.; Derby, J. J.; Godlevsky, V. V.; Jain, M.; Raty, J. Y.** (2001): Ab initio simulations of liquid semiconductors using the pseudopotential-density functional method. *J of Physics C*, vol. 13, pp. 817-854.
- Cohen, R. E.; Gong, Z.** (1994): Melting and melt structure of MgO at high pressures. *Physical Review B*, vol. 50, pp. 12301-12311.
- Flyvbjerg, H.; Petersen, H. G.** (1989): Error estimates on averages of correlated data. *J of Chemical Physics*, vol. 91, pp. 461-466.
- Hohenberg, P.; Kohn, W.** (1964): Inhomogeneous electron gas. *Physical Review*, vol. 136, pp. B864-B871.
- Horiuchi, H.; Ito, E.; Weidner, D.** (1987): Perovskite type MgSiO<sub>3</sub> single crystal X-ray diffraction study. *American Mineralogist*, vol. 72, pp. 357-360.
- Humphrey, W.; Dalke, A.; Schulten, K.** (1996): VMD - Visual Molecular Dynamics. *Journal of Molecular Graphics*, vol. 14, pp. 3-38.
- Karki B. B.; Bhattarai, D.; Stixrude, L.** (2006): First-principles calculations of the structural, dynamic and electronic properties of liquid MgO, *Physical Review B*, vol. 73, 174208.
- Khanduja, G; Karki, B. B.** (2005): Visualization of 3D

- scientific datasets based on interactive clipping. *The 13<sup>th</sup> Int. Conf. on Computer Graphics, Visualization and Computer Vision (WSCG 2005)*, ISBN 80-903100-9-5, pp. 59-66. 33-36.
- Khanduja, G.; Karki, B. B.** (2006): A systematic approach to multiple datasets visualization of scalar volume data. *The Int. Conf. on Computer Graphics Theory and Applications (GRAAP 2006)*, pp.
- Kohn, W.; Sham, L.** (1965): Self-consistent equations including exchange and correlation effects. *Physical Review*, vol. 140, pp. A1133-A1138.
- Kokaji, A.** (1999): XcrySDen – a new program for displaying crystalline structures and electron densities. *J of Molecular Graphics Modelling*, vol. 17, pp. 176-179.
- Kresse, G.; Furthmuller, J.** (1996): Efficiency of ab-initio total energy calculations for metals and semiconductors using a plane-wave basis set. *Computational Material Science*, vol. 6, pp. 15-50.
- Kresse, G., Hafner, J.; Needs, R. J.** (1992): Optimized norm-conserving pseudopotentials. *Journal of Physics C*, vol. 4, pp. 7451-7468.
- Lorensen, W. E.; Cline, H. E.** (1987): Marching cubes: a high-resolution 3D surface reconstruction algorithm. *Computer Graphics (Proc. of SIGGRAPH)*, vol. 21, pp. 163-169.
- Nose, S.** (1984): A unified formulation of the constant temperature molecular dynamics method. *J of Chemical Physics*, vol. 81, pp. 511-519.
- Rigden, S. M.; Ahrens, T. J.; Stolper, E. M.** (1984): Densities of silicate liquids at high pressure. *Science*, vol. 226, pp. 1071-1074.
- Sharma, A.; Haas, A.; Nakano, A.; Kalia, R.; Vashishta, P.; Kodiyalam, S.; Miller, P.; Zhao, W.; Liu, X.; Campbell, T. J.; Hass, A.** (2003): Immersive and interactive exploration of billion-atoms systems. *Presence*, vol. 12, pp. 85-95.
- Shen, S.; Atluri, S. N.** (2004): Computational nanomechanics and multi-scale simulation, *CMC: Computers, Materials & Continua*, vol. 1, pp. 59-90.
- Srivastava, D.; Atluri, S. N.** (2002): Computational nanotechnology: A current perspective, *CMES: Computer Modeling in Engineering & Sciences*, vol. 3, pp. 531-538.
- Stixrude, L.; Karki, B. B.** (2005): Structure and freezing of MgSiO<sub>3</sub> liquid in Earth's lower mantle. *Science*, vol. 310, pp. 297-299.
- Trave, A.; Tangney, P., Scandolo, S.; Pasquarello, A.; Car, R.** (2002): Pressure-induced structural changes in liquid SiO<sub>2</sub> from ab initio simulations. *Physical Review Letters*, vol. 89, No. 245504.
- Weiskopf D.; Engle, K.; Ertl, T.** (2003): Volume clipping techniques for texture-based volume visualization and volume shading. *IEEE Transactions on Visualization and Computer Graphic*, vol. 9, pp. 298-312.
- Zerr, A.; Boehler, R.** (1994): Constraints on the melting temperature of the lower mantle from high-pressure experiments on MgO and magnesioferrite. *Nature*, vol. 371, pp. 506-508.

